MDPI

Article

Design and Construction of a Device to Evaluate the Performance of Variable Orifice Flow Meters (VOFM)

William Prado Martínez [1],*, Juan Felipe Arroyave Londoño [2],* and Jefferson Vásquez Gómez [2]

1   Department of Mecathronics Engineering, Universidad Tecnológica de Pereira, Pereira 66001, Colombia
2   Department of Mechanical Tecnology, Universidad Tecnológica de Pereira, Pereira 66001, Colombia; jevasquez@utp.edu.co
*   Correspondence: prado@utp.edu.co (W.P.M.); jfa@utp.edu.co (J.F.A.L.)

Abstract: This work presents a low-cost device for evaluating Variable Orifice Flow Meters (VOFM) used in medical mechanical ventilation applications. Specifically, the equipment was used to assess the impact of length and thickness on pressure drop for different flows in a rectangular geometry VOFM. A total of six VOFMs, with three different lengths and two different thicknesses, were evaluated. All VOFMs were stimulated with an airflow ranging from 0 L.min^{-1} to 90 L.min^{-1}, with increments of approximately 2 L.min^{-1}. The experiments conducted with the device showed a strong relationship between pressure drop ΔP and flow rate Q in the evaluated VOFMs, with two different zones: one exhibiting non-linear behavior and another showing linear behavior. The results suggest that increased length and decreased thickness lead to higher sensitivity. However, it is essential to reduce the cross-sectional area to mitigate nonlinear effects of the sensor.

Keywords: variable orifice meter; flow meter; cantilever beam; flexible sensor

1. Introduction

Differential pressure flow meters are widely used devices for measuring fluid flow in pipelines due to their ease of installation and maintenance as well as their capability to measure different fluids. These devices operate based on the pressure drop when the fluid passes through a restriction [1], as shown in Figure 1.
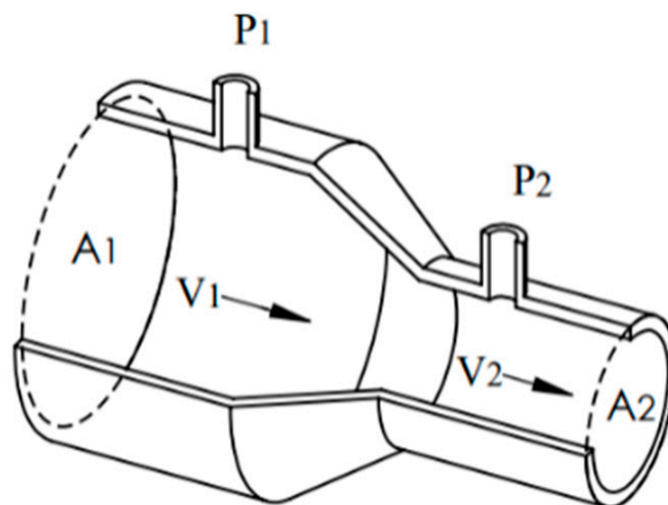

Figure 1. Restriction due to section change. Source: Authors.

According to the experiments, the fluid increases its velocity. It decreases its pressure as it passes through a reduced area, while it decreases its velocity and increases its pressure

if the area is increased. Equation (1), which relates the pressure drop $\Delta P = P_1 - P_2$ and the flow Q through the restriction in Figure 1, can be derived by applying the Bernoulli equation and the principle of mass conservation. This non-linear equation predicts that the flow is proportional to the square root of the pressure drop and has been widely used for flow measurement using devices with fixed area restrictions, such as the Venturi tube, fixed orifice plate, and nozzle:

$$Q = v_1 A_1 = \frac{A_2}{\sqrt{1 - \left(\frac{A_2}{A_1}\right)^2}} \sqrt{\frac{2}{\rho}} \sqrt{\Delta P} \tag{1}$$

where A_1 is the inlet area of the flowmeter, A_2 is the passage area of flow obstruction, and ρ is the fluid density.
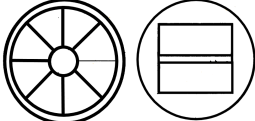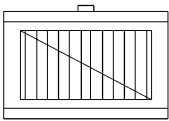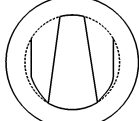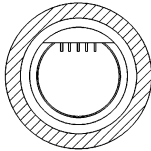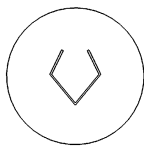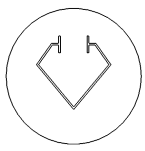
However, in industrial applications, deviations in measurement often arise due to factors such as flow profile and fluid properties, among others. Therefore, an experimentally determined correction coefficient is required, in addition to making adjustments related to the design, installation, and use of differential pressure meters to compensate for these deviations [2–4]. The abovementioned requirements are detailed in the ISO 5167-1 standard [5], establishing flow measurement standards in piping systems. The objective of this standard is to ensure the reliability of measurements.

In the case of medical applications, such as monitoring the respiratory function of patients connected to mechanical ventilation systems and anesthesia machines, flow meters with fixed area restrictions can generate a significantly high-pressure drop compared to the operating pressure [6,7]. This pressure drop results in an effort that hinders the efficient evacuation of gases from the patient during the expiratory phase, disrupting the respiratory cycle's naturalness [8]. This additional effort can make it challenging to obtain reliable and accurate measurements, which in turn hampers the ability of medical professionals to characterize the mechanical properties of the pulmonary system, understand the interaction between the patient and the mechanical ventilator, and accurately monitor changes in respiratory muscle activity [9–11]. On the other hand, an inaccurate measurement of flow can lead to inadequate patient ventilation therapy, which in the case of air and oxygen mixtures, can result in conditions such as irreversible pulmonary fibrosis and retrolental fibroplasia, among others [12]. Additionally, medical flow meters are susceptible to condensing moisture or secretions [13] and contamination by viruses and bacteria, which is why these meters must undergo strict sterilization processes for use on different patients or be limited to single-patient use, thereby increasing their cost [14,15].

The Variable Orifice Meter (VOFM) has been developed to reduce expiratory effort and cost. It has gained popularity due to its simplicity, robustness, low manufacturing cost, linear response, and ease of integration with electronic sensors and digital filters. The VOFM offers several advantages, including fast and accurate response, silent operation, and the ability to operate in a wide range of conditions, such as condensation or secretions in the gas flow exhaled by a patient [16,17]. The VOFM is a flexible membrane placed transversely in the respiratory circuit, with one or more cantilever beams cut on it. When the gas Q_{vofm} passes through the VOFM membrane, it creates a pressure drop ΔP that flexes the beams and increases the effective flow area. As a result, the expiratory effort is reduced.

A review conducted on Google Patents and Espacenet found approximately 40 patents related to VOFMs, of which nine, shown in Table 1, present claims that improve the linear relationship between Q_{vofm} and ΔP. The simplest reported shape is the rectangular geometry, while the geometry with the most operating claims is the rhomboidal geometry.

Table 1. Displays the beam shapes used in the patents.

Multiple beams				
US9931056B2	US4006634A	US3989037A	US4989456A	

Single beam			
US5970801A	US4083245	EP-0331773A1	US10905357B2

The patent US4083245 [18] details that the rhomboidal shape of the beam generates a more linear relationship between pressure drop and flow than other shapes, such as rectangular or circular [19]. This means that a differential pressure gauge can indicate the flow, which is advantageous in measurement directly. On the other hand, patents US4006634A [20] and US4989456A [21] argue that using a single beam instead of multiple beams significantly reduces the noise present in the designs due to vibration and resonance effects. Regarding the location of the pressure taps, patent US4006634A states that they should be placed on the side of the beam's fixed end to avoid affecting the measurement due to gas vortices or other unwanted effects that could distort the pressure reading and consequently affect the accuracy. Table 2 presents the type of material and thickness stated in each invention. The use of Mylar® (biaxially oriented polyethylene terephthalate) is common in several of the mentioned patents due to its beneficial characteristics such as dimensional stability, flatness, chemical resistance, fatigue resistance, and heat resistance up to 230 °C, good electrical resistance, and adequate mechanical strength [22–24]. Mylar® is commercially available in thicknesses ranging from 0.001 inches to 0.014 inches.

Table 2. Proposed materials in patents for VOFMs.

Patent	Material	Thickness
US4083245A	Synthetic rubber	0.9 mm
US4006634A	Material with Young's modulus 3×10^7 psi	-
US9931056B2 [25]	Flexible material	-
US3989037A [26]	Polymer	0.05 mm
EP0331773A1	Mylar®	50 µm y 125 µm
US5970801A	Metallic	-
US4989456 A	Stainless steel series 300	0.0254 mm (0.001 in)
US7798016B2	Mylar®	0.1 mm–0.15 mm
US10905357B2	Mylar®	0.127 mm–0.1778 mm (0.005 in–0.007 in)

Despite the extensive development of VOFM, the technical and scientific literature does not report experiments evaluating the impact of the length and thickness of the VOFM beam on its response. Therefore, this work proposes the construction of a device to assess the influence of beam length and thickness on the behavior of a variable orifice meter for medical applications. The design of the device and the experimental results obtained for six rectangular VOFM designs will be presented.

Theoretical Flow Rate Q

The theoretical flow rate Q considered in this work corresponds to the calculation based on Equation (1) for an incompressible fluid flowing through a restriction without considering energy losses due to fluid conditions or restriction geometry [27]. The pressure difference exerts a force per unit length on the cantilever beam, resulting in its deflection. The greater the deflection of the beam, the larger the opening area for gas flow. Additionally, the deflection model [28] of a beam with a distributed load due to steady fluid flow [29], as employed in this work with the rectangular configuration shown in Figure 2, is calculated from Equation (2), which predicts deflection as a function of pressure drop:

$$y = \frac{3L^4}{2Ee^3} \Delta P \tag{2}$$

where *B* is the width at the support, *L* the length, *e* the thickness, *I* the moment of inertia, *E* the elastic modulus, and *t* cutting thickness, as shown in Figure 2a,b.

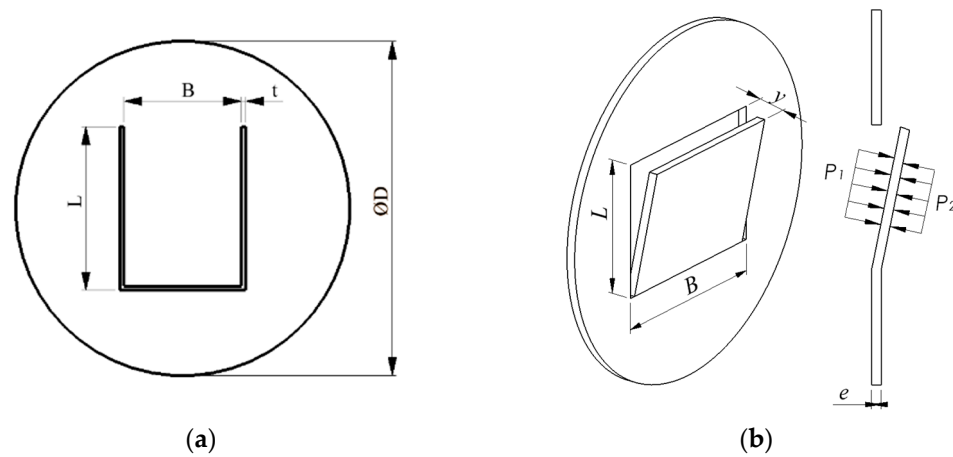| (**a**) | (**b**) |

Figure 2. Variable orifice flow meter: (**a**) geometry of variable orifice flow meter; (**b**) deflected beam. Source: Authors.

According to Figure 2b, the opening area A_2 can then be calculated by adding to the area of the cut $A_e = (2L + B)t$ and the increment of the area due to deflection, as shown in Equation (3):

$$A_2 = \sqrt{\left[(2L + B)\, t \right]^2 + \left[(B + L)\frac{3L^4}{2Ee^3} \Delta P \right]^2} \tag{3}$$

Therefore, Equation (4) for the predicted theoretical flow rate Q for the VOFM can be derived as follows:

$$Q = \frac{\sqrt{\left[(B + L)\frac{3L^4}{2Ee^3} \Delta P \right]^2 + \left[(2L + B)\, t \right]^2}}{\sqrt{1 - \left(\frac{\sqrt{\left[(B+L)\frac{3L^4}{2Ee^3} \Delta P \right]^2 + \left[(2L+B)\, t \right]^2}}{A_1} \right)^2}} \sqrt{\frac{2}{\rho}} \sqrt{\Delta P} \tag{4}$$

2. Measurement System

Taking into account the flow and pressure variables described in the models for evaluating the behavior of beams in variable orifice flow meters, we have designed and developed a comprehensive measurement system. This system comprises a gas circuit with a container specially designed to secure the beam of the plates. Additionally, an electronic system dedicated to the accurate reading of the sensors and actuator control has been implemented. To ensure effective data tracking and timely storage, we have

incorporated a software platform that enables continuous monitoring and capturing of relevant information.

Furthermore, given that the VOFM is intended for medical use, design considerations for the measurement system were based on the guidelines provided by the National Institute of Food and Drug Surveillance of Colombia (INVIMA), which include the following: the mechanical ventilation conditions [30,31], recommendations from Colombian scientific societies [32,33], international health agencies [34–36], and the guidelines provided by the World Health Organization (WHO) [37].

Figure 3 shows the device to Evaluate the Performance of Variable Orifice Flow Meters (VOFM) used in this work, which consists of a gas circuit with a container housing the VOFM, an electronic system for sensor reading and actuator control, and software for data monitoring and storage.
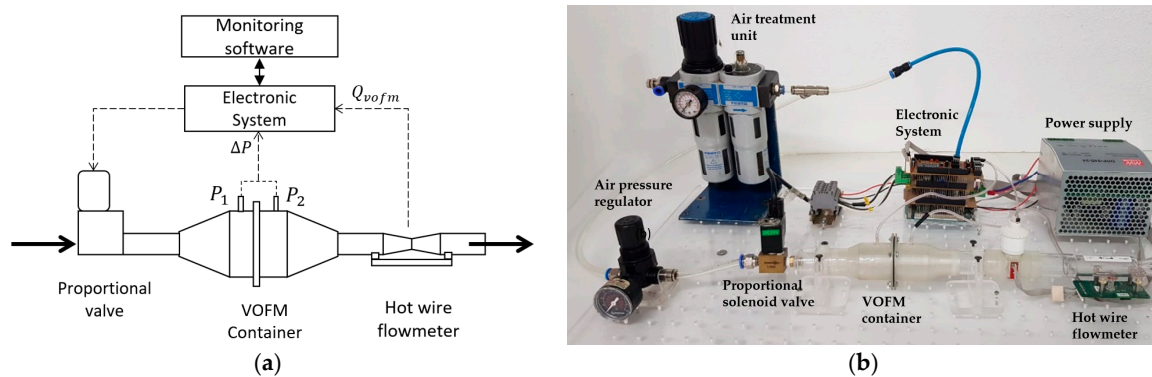

Figure 3. Measurement device: (**a**) schematic of a measurement device; (**b**) experimental setup. Source: Authors.

2.1. Gas Circuit

The gas from a compressed air network is regulated into the VOFM container using a proportional solenoid valve. Then, the gas flows into container (b), where the pressure taps are located, P_1 and P_2.

The VOFM container, depicted in Figure 4, was designed using two symmetrical cone-shaped parts. According to patent EP-0331773A1 [38], the cone angle is set at 23.61°. A flanged connection and an O-ring gasket ensure the container's airtightness. The positioning of the pressure taps on the upper section of the container enables the VOFM to measure bidirectional flow effectively, unaffected by condensation and the downward orientation of the VOFM beam which reduces the effects of turbulence on the pressure taps. The container was fabricated using 3D printing technology and medical-grade resin.
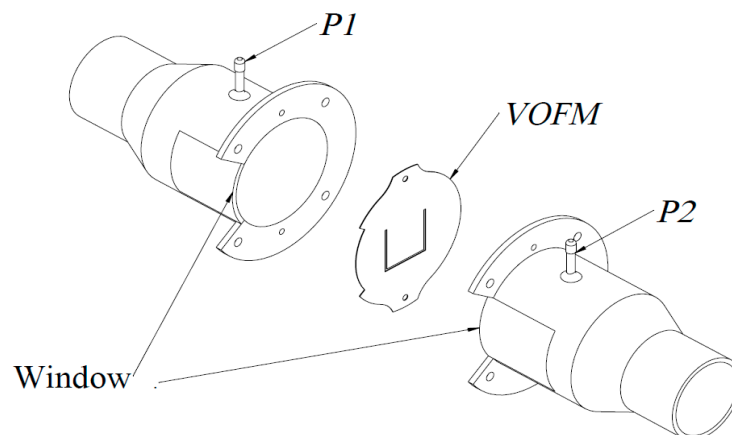

Figure 4. VOFM Container. Source: Authors.

2.2. Electronic System

The electronic system was developed using an Arduino Due® and three PCBs (Printed Circuit Boards) designed and manufactured in the Universidad Tecnológica de Pereira. The Arduino Due® and the three boards connected in a four-level arrangement, as shown in Figure 5a. The Arduino Due processing board (b) is responsible for processing sensor information, establishing communication with the data acquisition software, and controlling the operation sequence.
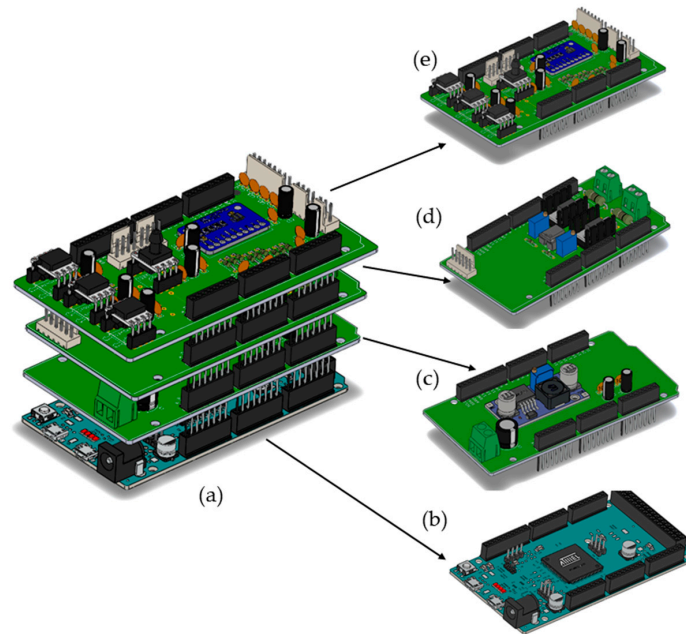

Figure 5. Electronic system: (**a**) four-level arrangement: (**b**) Arduino Due processing board for processing information, communication, and controlling the operation sequence; (**c**) power board; (**d**) proportional valve control board; (**e**) instrumentation board. Source: Authors.

The power board (c) regulates the voltage levels of 3.3 V and 5 V that power the sensors from a 24 V 5A switch-type power supply.

On board (d), the proportional valve control circuit is situated, comprising an LM358 operational amplifier and a TIP120 transistor. This circuit governs the proportional valve's opening Yongchuang YCLT21-1GBVV-SC11. For this purpose, the control circuit regulates the current flowing through the coil based on the analog voltage signal DAC0, ranging from 0 V to 3.3 V, supplied by the Arduino Due, as illustrated in Figure 6.
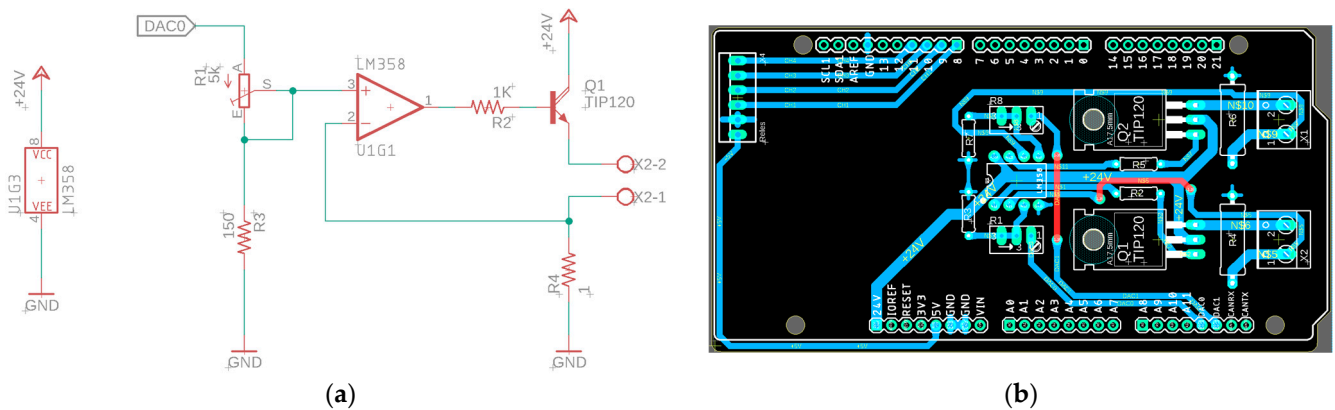

(**a**) (**b**)

Figure 6. Control circuit for the proportional solenoid valve: (**a**) electronic diagram of proportional solenoid valve; (**b**) PCB of the control circuit for the proportional solenoid valve. Source: Authors.

The proportional valve Yongchuang YCLT21-1GBVV-SC11 operates with a maximum coil current of 270 mA at Full Scale (FS) based on a power calculation of 6.5 W and a voltage of 24 VDC. When subjected to a supply pressure of 400 kPa (58 psi) and a current of 85% FS (230 mA), the resulting flow rate from the proportional valve is approximately 110 ± 10 L.min^{-1}. Additionally, under the same supply pressure, the minimum current required to initiate the valve's proportional opening is approximately 30% FS (80 mA).

The instrumentation board (e) is designed to connect a differential pressure sensor SPD1 to measure the pressure drop ΔP across the VOFM and a hot wire flow meter TSI to measure the Q_{vofm} with port X4-1 and gas temperature T with port X4-2.

The circuits on the instrumentation board, as shown in Figure 7, demonstrate the use of 0.1 uF capacitances to filter out high-frequency signals that could affect the measurements. The differential pressure sensor SPD2 in Figure 7c, to which the P_1 and P_2 pressure taps of the VOFM are connected, is the SSCDRRN100MDAA5 model, which has an operating range of ± 10 kPa (± 1.45 PSI) with an accuracy of 0.25% [19]. The PCB in Figure 7d displays three circuits similar to those in Figure 7c. In SPD1 and SPD4, a 3.3 V-supplied differential pressure sensor can be installed as a backup in case of SPD2 failure. In SPD3, an HSCMANN100PGAA3 sensor was installed to measure the supply pressure to the proportional valve, which has an operating range of 0 kPa to 689.5 kPa (0 PSIG–100 PSIG). On the other hand, the hot wire flowmeter used as a reference instrument is a TSI-840120 Rev:E model with an accuracy of $\pm 2.5\%$ of the reading.
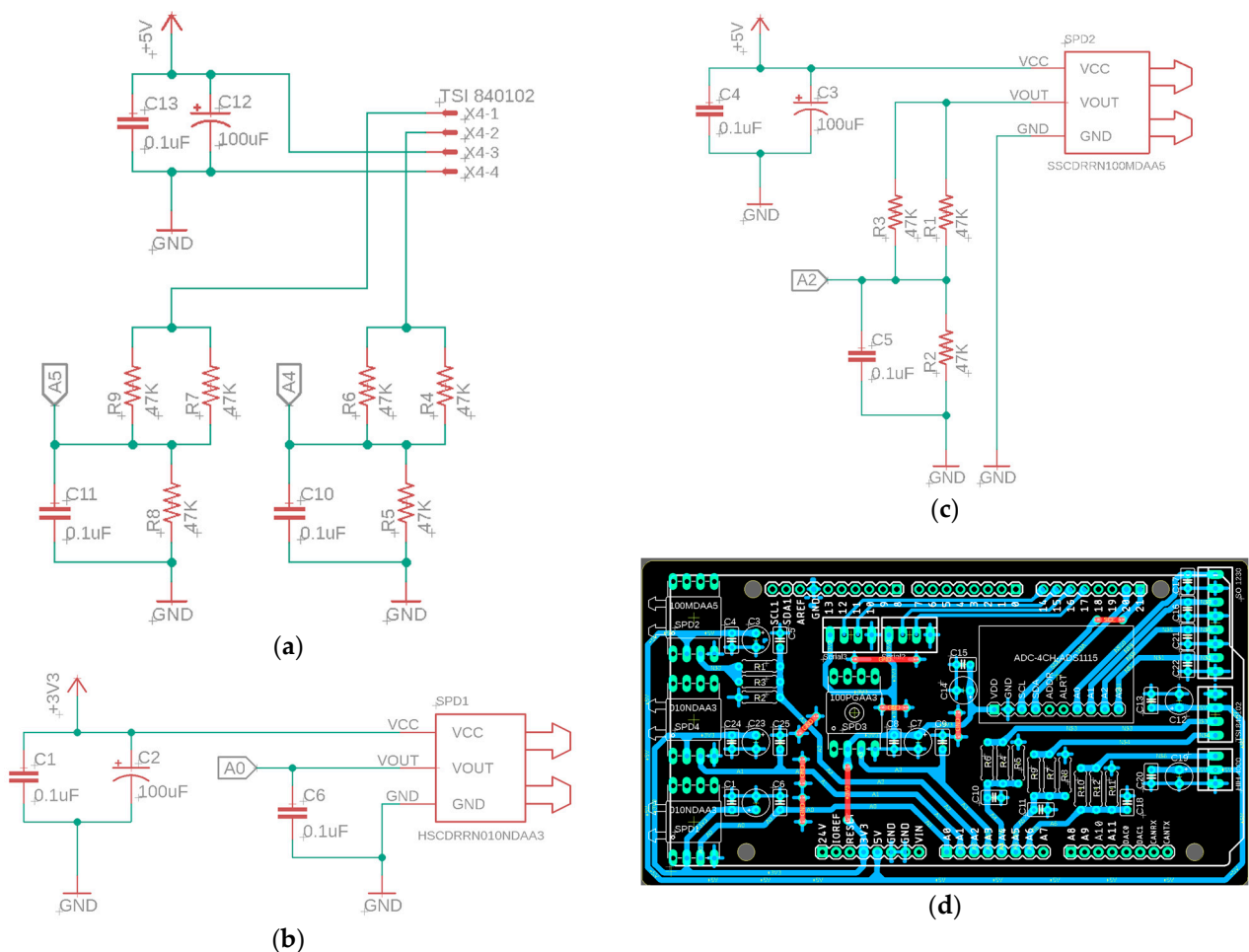
Figure 7. Circuit for the pressure sensors: (**a**) electronic diagram to hot wire flowmeter; (**b**) electronic diagram to pressure sensors SPD1 and SPD4; (**c**) electronic diagram to pressure sensor SPD2; (**d**) PCB for the pressure sensors and hot wire flow meter. Source: Authors.

A program for Arduino Due corrects the flow error caused by temperature, oxygen (O2) percentage in the air, and electrical noise. This program is based on the correction equation provided by the manufacturer of the hot wire sensor and incorporates an averaging filter routine that takes 20 flow measurements. The flow error is calculated as $E_Q = Q_{sp} - Q_{vofm}$, where Q_{sp} is SetPoint flow value or desired flow value; it is used by a PID algorithm implemented on the Arduino Due to correct the errors by comparing the actual flow value measured by the hot wire sensor.

2.3. Monitoring Software

Lastly, a SCADA interface was developed using Indusoft Web Studio Educational® 8.1 software to operate the device and store the data. The software was installed on a laptop with the following specifications: Intel Core i5, 8 GB RAM, and 512 GB SSD storage. An RS232 serial communication between the Arduino Due and the application hosted on a computer was implemented. The communication driver allows receiving sensor measurement information at a baud rate of 115,200 bps. The driver also enables parameterizing the SetPoint flow value to be delivered by the proportional valve. Figure 8 shows the adjustment parameters, the selection buttons for MANUAL or AUTOMATIC operation, and the readings from the sensors on the developed interface.

Figure 8. Monitoring software interface. Source: Authors.

If the behavior of a VOFM is to be evaluated, the MANUAL operation mode is selected in the SCADA. In this mode, it is necessary to provide the parameters (inspiration time T_i, respiratory rate (FR), maximum inspiratory pressure (PIP), positive end-expiratory pressure (PEEP), and tidal volume (Vc) to calculate the desired flow value for a proportional valve opening. Simultaneously, the information collected (pressure drop across the MOV, supply network pressure, gas temperature, humidity, O2 percentage, and the hot-wire meter flow value) by the monitoring software is stored in a TXT file as a historical record of the system's operation so that it can be subsequently used by other software or databases.

If the operation of a mechanical ventilation system is to be simulated, the AUTOMATIC operation mode is selected. This mode corresponds to constant-flow ventilation, limited by pressure and cycled by time.

3. Experiment

With the aim of assessing the performance of the VOFM, air coming from the proportional valve was passed through the VOFM to record the pressure drop and, subsequently, through the wire flow meter to determine the flow. In total, six variable orifice flow meters were evaluated, which were cut on Mylar sheets according to a factorial design. This design considered a width $B = 15$ mm with three different lengths ($L1 = 15$ mm, $L2 = 19.5$ mm, and $L3 = 22.5$ mm) and two different thicknesses ($e1 = 0.1016$ mm and $e2 = 0.1905$ mm). All VOFMs were stimulated with an airflow ranging from 0 L.min^{-1} to 90 L.min^{-1}, with increments of approximately 2 L.min^{-1}. For each airflow value Q_{vofm}, a total of $n = 20$ repetitions of the pressure drop ΔP across the VOFM were recorded. The fluid used was air with an oxygen percentage of approximately 21% and with a temperature during the experiments of 25 °C $\pm$ 2 °C.

The measure of dispersion $S_{\Delta P}$ of the pressure drop ΔP was calculated using Equation (5):

$$S_{\Delta P} = \sqrt{\frac{\sum \left(\Delta P - \overline{\Delta P}\right)^2}{n - 1}} \tag{5}$$

The deflection of the beam in the VOFM was validated by measuring the deflection using images and comparing the results with the theoretical deflection.

4. Results

4.1. Pressure Drop and Deflection

Since Equation (2) predicts that the deflection of the beam is directly proportional to the pressure drop, an experiment was conducted to experimentally evaluate this relationship in a beam with dimensions $A1 = 15$ mm and $L2 = 19.5$ mm. For this purpose, the deflection of the beam y_r was measured using images as shown in Figure 9, and it was compared with the theoretical deflection y from Equation (2).
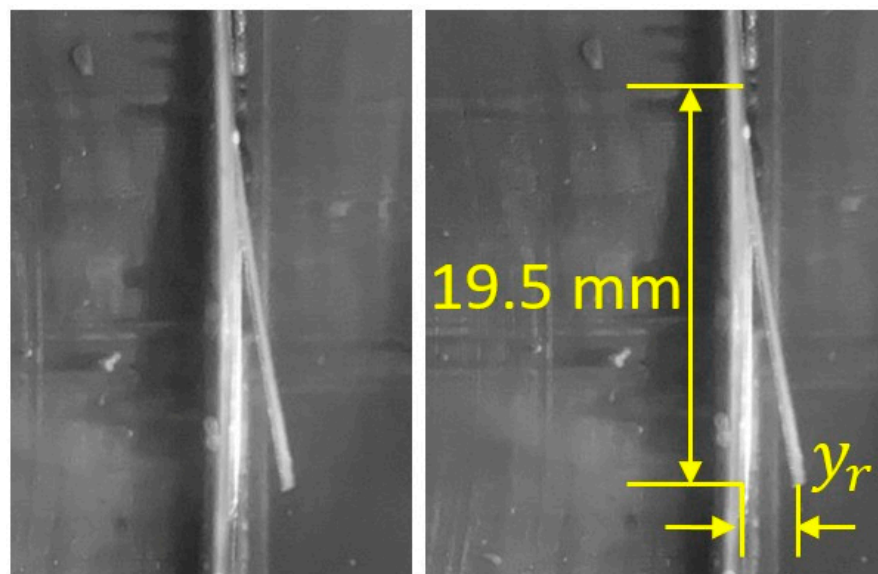
Figure 9. Photograph of the beam deflection. Source: Authors.

The results in Table 3 show that, for $Q_{vofm} \geq 31.0$ L.min^{-1}, the error between the measured and calculated deflection is less than 5.4%, while, for $Q_{vofm} \leq 21.3$ L.min^{-1}), the error is higher than 5.4%. Typically, mechanical ventilation equipment for medical applications passes flow calibration tests if the error is below 10%.

Table 3. Results of the beam deflection.

Q_{vofm} (L.min^{-1})	ΔP (Pa)	y_r (mm)	y (mm)	Error
4.2	0.4	0.1	0.004	95.6%
11.9	13.8	0.2	0.167	16.6%
21.3	40.3	0.4	0.489	22.2%
31.0	69.5	0.8	0.843	5.4%
40.6	102.3	1.2	1.241	3.4%
51.2	129.7	1.5	1.573	4.8%
61.2	158.8	1.9	1.926	1.4%
71.6	189.4	2.2	2.298	4.4%
81.2	230.2	2.7	2.792	2.6%
89.3	252.7	3.1	3.065	1.1%

4.2. Relationship between Pressure Drop ΔP and Flow Rate Q_{vofm}

Figure 10a displays the results obtained for three lengths of a beam with thickness $e1 = 0.1016$ mm, while Figure 10b shows the results for a thickness of $e2 = 0.1905$ mm. In the mentioned figures, it is evident that at low flows, the pressure drop with respect to flow is not linear, while if the flow is increased, the behavior becomes linear.
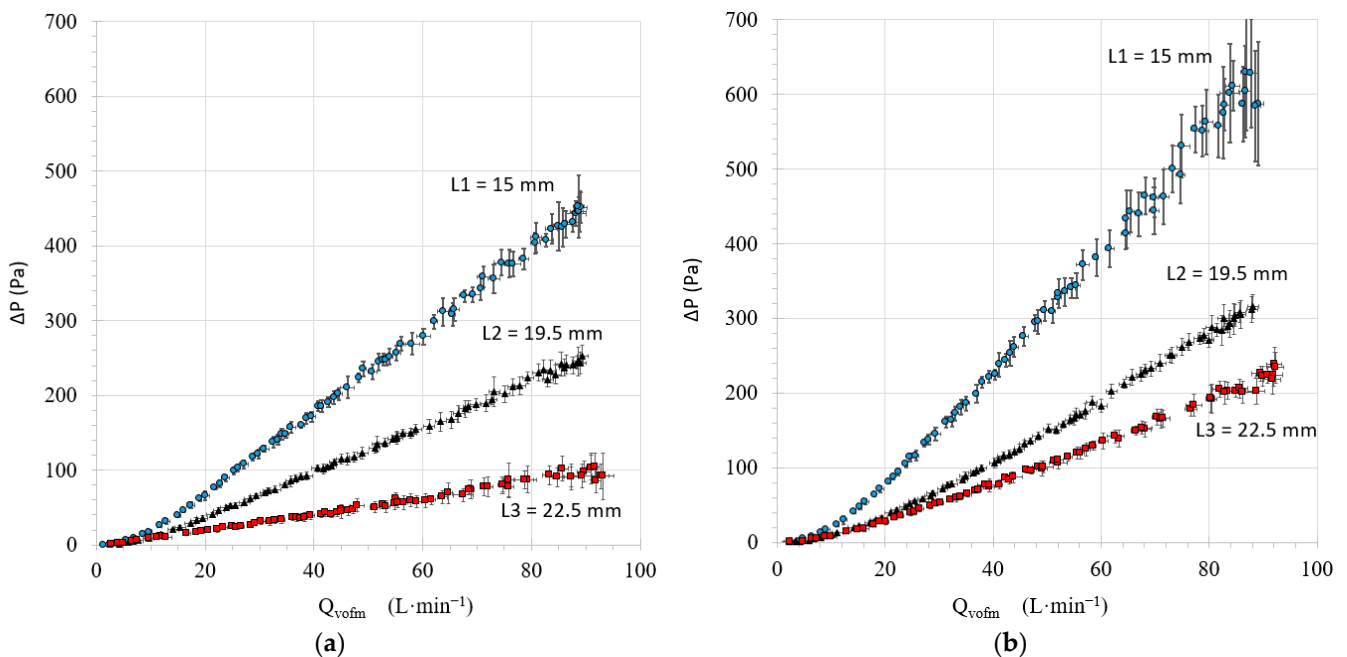

Figure 10. Results for three lengths of a beam pressure drop ΔP and flow rate Q_{vofm}: (**a**) thickness $e1 = 0.1016$ mm; (**b**) thickness $e2 = 0.1905$ mm. Source: Authors.

The transition between linear and non-linear behaviors was obtained through linear regression analysis and residual error analysis. For linear regression, a mathematical model of the form $\overline{\Delta P} = \gamma_0 + \gamma_1 Q_{vofm}$, was used, and a set of data far from the non-linear region was considered. In this case, we considered the data for which $Q_{vofm} \geq 30$ L.min^{-1}. Tables 4 and 5 show an R^2 close to one for all dimensions, indicating that the mathematical model predicts a strong relationship between the pressure drop and the flow.

Table 4. Linear regression for thickness $e1 = 0.1016$ mm.

A (mm)	L (mm)	γ	γ_0	R^2
15	15	5.5045	-43.74464	0.9990
15	19.5	3.0528	-24.75242	0.9989
15	22.5	1.1228	-4.981751	0.9892

Table 5. Linear regression for thickness $e2 = 0.1905$ mm.

A (mm)	L (mm)	γ	γ_0	R^2
15	15	8.0832	-95.399	0.9962
15	19.5	4.3410	-67.639	0.9988
15	22.5	2.8709	-38.435	0.9969

Figure 11 shows the residual error $Er = \Delta P - \overline{\Delta P}$, where ΔP is the experimental pressure drop and y $\overline{\Delta P}$ is the expected value from the regression. The transition to linear behavior is depicted in Figure 11 with dashed vertical lines. On the left side of the lines, the behavior of ΔP with respect to Q_{vofm} is non-linear and similar to gas flow behavior through a fixed orifice plate.
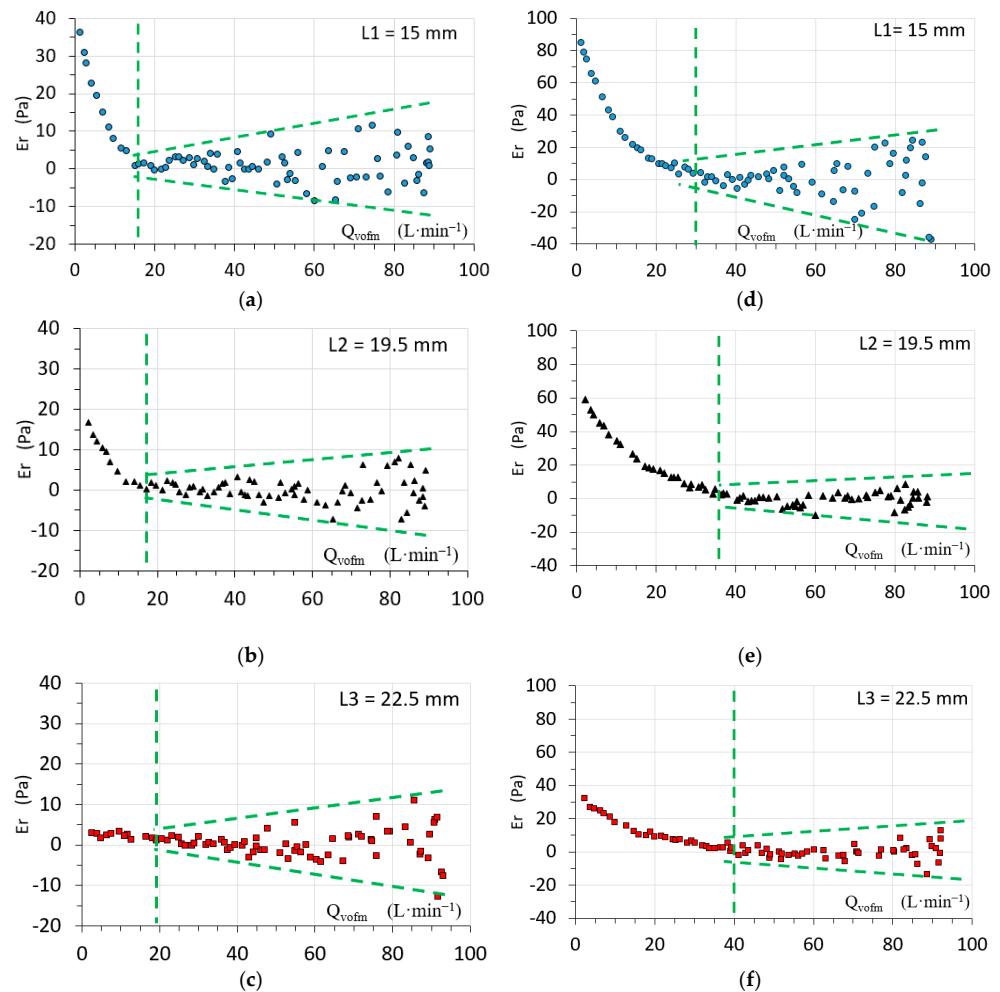

Figure 11. Residual errors for VOFMs with different lengths and thickness: (**a–c**) with a thickness $e1 = 0.1016$ mm; (**d–f**) with a thickness $e2 = 0.1905$ mm. Source: Authors.

On the right side, the linear regression model exhibits increasing heteroscedasticity. This behavior is associated with turbulent flow regimes that increase variance. Table 6 presents the transition flow values obtained from Figure 11, where the transition between the non-linear and linear zones occurs. Figure 12 shows the transition flow rate as a function of the area A_e.

Table 6. Transition flows.

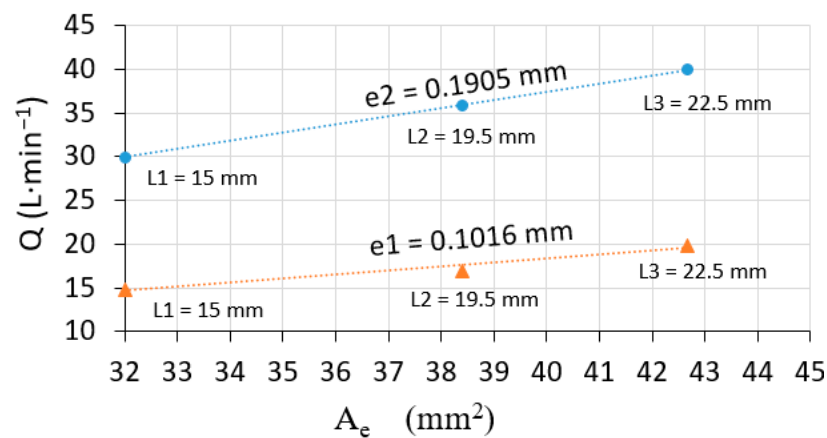|	e1 = 0.1016 mm	e2 = 0.1905 mm
L1 = 15 mm	15 L.min^{-1}	30 L.min^{-1}
L2 = 19.5 mm	17 L.min^{-1}	36 L.min^{-1}
L3 = 22.5 mm	20 L.min^{-1}	40 L.min^{-1}

Figure 12. Transition flow as a function of A_e. Source: Authors.

5. Discussion

Considering the previous results, we can now identify more clearly how the length of the VOFM beam influences the pressure drop behavior at different flows. The experiments show two zones: a non-linear zone and a linear behavior zone. In the non-linear zone, which is present at low flows, the pressure difference exerted on the plate is insufficient to overcome the material stiffness, meaning that gas flows through the area of the cut slots $A_e = (2L + B)t$ without causing appreciable deflection. As a result, the pressure drop at low flows in the variable orifice meter is proportional to the square of the flow rate, similar to the behavior of a fixed orifice plate.

The area A_e can be significantly reduced by reducing the thickness of the cut slot t more than by variations in L o B because of the following:

$$\frac{\partial A_e}{\partial t} \gg \frac{\partial A_e}{\partial L}$$

The transition flow is also affected by the thickness. According to the deflection equation for a cantilever beam, the stiffness of the beam increases as its thickness increases. An increase in the thickness of the VOFM results in less deflection and a smaller opening for fluid passage, increasing the flow resistance. Therefore, a higher flow is required for the transition if the thickness is increased. This finding highlights the importance of thickness in the design and operation of variable orifice meters.

Even though the linear regression model showed values close to one for the coefficient of determination R^2, the measure of dispersion $S_{\Delta P}$ of the measurements increased proportionally with the flow rate, indicating that the errors are not constant. This suggests that the obstruction generates vortices and turbulence through the orifice plate. These vortices and turbulence affect the velocity distribution and flow structure, which can modify the Reynolds number in the region near the orifice plate.

We calculated the Reynolds number for the circular pipe upstream of the VOFM us-ing the equations for a circular section to verify any potential turbulence influence that could affect the VOFM beam. According to the Reynolds number, we found that, at a flow rate of around 35 L.min^{-1}, the transition from laminar to turbulent flow begins, and at a flow rate of 67 L.min^{-1}, the flow regime will be turbulent. For this reason, we can assert that the increased variance in the pressure drop is due to the flow regime. However, we did not calculate the Reynolds number directly at the VOFM section. Therefore, we consider it important to design mathematical models and conduct experiments to assess the flow regime precisely at the VOFM, considering the variable geometry. This would enable the optimization of the VOFM beam geometries for potential plate vibrations and, thus, enhance its accuracy as a flow measurement sensor.

For this reason, we can assert that the increased variance in pressure drop is due to the flow regime. However, we did not calculate the Reynolds number directly at the VOFM section. Therefore, we consider it important to design mathematical models and conduct experiments to assess the flow regime precisely at the VOFM, considering the variable geometry. This would enable the optimization of the VOFM beam geometries for potential plate vibrations and, thus, enhance its accuracy as a flow measurement sensor.

With the device, we have discovered that increasing the length of the beam and reducing its thickness can enhance sensitivity. However, geometry changes need to be adjusted according to the requirements of mechanical ventilation. This is crucial because the treatment for mechanical ventilation varies significantly between patients such as human neonates and adults. This is even more critical if the VOFM is applied to pets or animals, as the variability in ventilation requirements is extensive.

6. Conclusions

This study has introduced an innovative, cost-effective device specifically designed for the assessment of Variable Orifice Flow Meters (VOFM) of the beam type, commonly used in medical mechanical ventilation applications. The device consists of three mod-ules: an experimental setup, an electronic control board for data acquisition and control of the equipment, and software for running the system and processing data using SCADA.

The measurement device can record the following: the supply pressure from 0 to 100 psi; the gas temperature from 0 °C to 50 °C; the oxygen concentration from 0 to 100%; the relative hu-midity from 0 to 100%; the pressure drops across the plate from −0.1 bar to 0.1 bar; gas flow rate from 0 to 100 L.min^{-1}; and the proximal pressure to the patient from −0.1 bar to 0.1 bar. On the other hand, software parameterization allows the simulation of operating conditions of a mechanical ventilator for living beings by defining parameters such as inspiration time (Ti), tidal volume (Vi), and respiratory frequency (FR).

This devised system and its methodological approach have demonstrated their efficacy as invaluable tools for the precise and systematic evaluation of Variable Orifice Flow Meters in medical applications. The findings not only enhance our understanding of the factors influencing pressure drop in these configurations but also hold vital implications for the optimization and design of mechanical ventilation systems.

Finally, to utilize VOFM in mechanical ventilation and functional respiratory monitor-ing, it is necessary to perform the following: investigate the impact of various geometries, minimize turbulence formation in the orifice plate, and utilize digital signal filtering tech-niques for pressure signals.

References

1. Hardy, J.E.; Hylton, J.O.; McKnight, T.E.; Remenyik, C.J.; Ruppel, F.R. *Flow Measurement Methods and Applications*; John Wiley & Sons: Hoboken, NJ, USA, 1999; ISBN 978-0-471-24509-4.
2. Baker, R.C. *Flow Measurement Handbook: Industrial Designs, Operating Principles, Performance, and Applications*; Cambridge University Press: Cambridge, UK, 2000.
3. Shustrova, M.; Fafurin, A.; Baytimirov, A. The Question of Dynamic Gas Flow Measuring. In Proceedings of the 2019 International Conference on Industrial Engineering, Applications and Manufacturing (ICIEAM), Sochi, Russia, 25–29 March 2019; pp. 1–6.
4. Tomaszewska-Wach, B.; Rzasa, M. A Correction Method for Wet Gas Flow Metering Using a Standard Orifice and Slotted Orifices. *Sensors* **2021**, *21*, 2291. [CrossRef] [PubMed]
5. *BS EN ISO 5167-1*; Measurement of Fluid Flow by Means of Pressure Differential Devices Inserted in Circular Cross-Section Conduits Running Full: Part 1. General Principles and Requirements. British Standards Institution: London, UK, 2021.
6. Chavarri, J.A.C.; Ruiz, C.G.R.; Gómez Amador, A.M.; Cardenas, B.J.M.A.; Anaya, S.C.; Lozano Jauregui, J.H.; Hinostroza, A.T.; Jiménez de Cisneros y Fonfría, J.J. Mathematical Analysis of a Low Cost Mechanical Ventilator Respiratory Dynamics Enhanced by a Sensor Transducer (ST) Based in Nanostructures of Anodic Aluminium Oxide (AAO). *Mathematics* **2022**, *10*, 2403. [CrossRef]
7. Kudrna, P. Effects of Orifice Plate as a Flow Sensor in an Endotracheal Tube on the Ability of Elimination CO_2 during HFJV—Animal Study. *Appl. Sci.* **2021**, *11*, 4210. [CrossRef]
8. Kwon, J.; Kang, E.; Shin, S.; Lee, B.; Ko, M.; Kim, S.; Lee, S. Ventilation Difficulty Caused by Obstructed Heated Breathing Circuit. *Medicina* **2023**, *59*, 965. [CrossRef] [PubMed]
9. Vales, S.B.; Gómez, L.R. *Fundamentos de la Ventilación Mecánica*; Marge Books: Barcelona, Spain, 2023; ISBN 978-84-15340-50-8.
10. Eckhout, G.V.; Bhatia, S. Another Cause of Difficulty in Ventilating a Patient. *J. Clin. Anesth.* **2003**, *15*, 137–139. [CrossRef] [PubMed]
11. Nicolò, A.; Massaroni, C.; Schena, E.; Sacchetti, M. The Importance of Respiratory Rate Monitoring: From Healthcare to Sport and Exercise. *Sensors* **2020**, *20*, 6396. [CrossRef] [PubMed]
12. Duprez, F.; Barile, M.; Bonus, T.; Cuvelier, G.; Ollieuz, S.; Mashayekhi, S.; Legrand, A. Accuracy of Medical Oxygen Flowmeters: A Multicentric Field Study. *Health* **2014**. [CrossRef]
13. Kazmina, A.S.; Makukha, V.K. Testing of the Airflow Sensor Honeywell AWM42300V for Using It in Spirometer. In Proceedings of the 2017 IEEE Conference of Russian Young Researchers in Electrical and Electronic Engineering (EIConRus), St. Petersburg and Moscow, Russia, 1–3 February 2017; pp. 36–39.
14. Pintavirooj, C.; Maneerat, A.; Visitsattapongse, S. Emergency Blower-Based Ventilator with Novel-Designed Ventilation Sensor and Actuator. *Electronics* **2022**, *11*, 753. [CrossRef]
15. Chen, X.; Liu, C.; Yang, D.; Liu, X.; Hu, L.; Xie, J. Highly Accurate Airflow Volumetric Flowmeters via PMUTs Arrays Based on Transit Time. *J. Microelectromech. Syst.* **2019**, *28*, 707–716. [CrossRef]
16. Tardi, G.; Massaroni, C.; Saccomandi, P.; Schena, E. Experimental Assessment of a Variable Orifice Flowmeter for Respiratory Monitoring. *J. Sensors* **2015**, *2015*, e752540. [CrossRef]
17. Montagna, F.; Schena, E.; Massaroni, C.; Caciotti, C.; Presti, D.L.; Silvestri, S. Influence of the Length of Lead Lines on the Response of a Variable Orifice Meter: Analysis of Sensitivity and Settling Time. In Proceedings of the 2018 IEEE International Symposium on Medical Measurements and Applications (MeMeA), Rome, Italy, 11–13 June 2018; pp. 1–6.
18. Osborn, J.J. Variable Orifice Gas Flow Sensing Head. U.S. Patent US4083245A, 11 April 1978.
19. Ciobanu, C.I.; Schaeffer, D. Variable Orifice Flow Sensor. U.S. Patent US5970801A, 26 October 1999.
20. Billette, R.J.; Zias, A.R. Flow Meter. U.S. Patent US4006634, 8 February 1977.
21. Stupecky, J. Variable Area Obstruction Gas Flow Meter. U.S. Patent US5038621A, 13 August 1991.
22. Beer, R.H.M.D.; Kuypers, M.H.; Holland, J.; Schotte, H. Flow Resistance Tube for Gas Flow Meter. E.P. Patent EP0331772A1, 13 September 1989.
23. Bonassa, J. Flow Sensor with Double Obstruction. U.S. Patent US20090064794A1, 21 September 2010.
24. Friberg, H.; Daescher, J. Respiratory Flow Sensor. U.S. Patent US10905357B2, 2 February 2021.
25. Ganseman, J.; Ayoubi, A.; Ayoubi, N.; Bellaire, T.; Brodkin, I.; Dosil, V.; Findlay, J.; Halwani, F.; Willms, A. Spirometer Breathing Tube with Compound Membrane. U.S. Patent CA2803645A1, 5 January 2012.
26. Franetzki, M. Flow Measuring Device. U.S. Patent US3989037, 2 November 1976.
27. Funaki, T.; Kawashima, K.; Fujita, T.; Kagawa, T. Characteristic Analysis of Variable Orifice Flow Meter. *Proc. JFPS Int. Symp. Fluid Power* **2002**, *2002*, 83–88. [CrossRef]
28. Wang, Q.; Cui, J.; Tang, Y.; Pang, L.; Chen, K.; Zhang, B. Research on a Precision Calibration Model of a Flexible Strain Sensor Based on a Variable Section Cantilever Beam. *Sensors* **2023**, *23*, 4778. [CrossRef] [PubMed]
29. Ruan, C.; Chen, M.; Yu, Y.; Zhang, Y.; Wang, J.; Zhang, Z.; Yang, J.; Zhu, S.; Qu, B. Research on Very-Low-Frequency Hydroacoustic Acoustic Velocity Sensor Based on DFB Fiber Laser. *Photonics* **2023**, *10*, 463. [CrossRef]

30. Gutiérrez Muñoz, F. Ventilación Mecánica. *Acta Médica Peru.* **2011**, *28*, 87–104.
31. Williams, D.; Flory, S.; King, R.; Thornton, M.; Dingley, J. A Low Oxygen Consumption Pneumatic Ventilator for Emergency Construction during a Respiratory Failure Pandemic. *Anaesthesia* **2010**, *65*, 235–242. [CrossRef] [PubMed]
32. Capítulo 7. Manejo Del Paciente COVID-19 en UCI. Available online: https://amci.org.co/images/consenso/Capitulo_7_Manejo_del_paciente_COVID-19_en_UCI.pdf (accessed on 10 May 2023).
33. Chica-Meza, C.; Peña-López, L.A.; Villamarín-Guerrero, H.F.; Moreno-Collazos, J.E.; Rodríguez-Corredor, L.C.; Lozano, W.M.; Vargas-Ordoñez, M.P. Cuidado respiratorio en COVID-19. *Acta Colomb. Cuid. Intensivo* **2020**, *20*, 108–117. [CrossRef]
34. Información Sobre Prototipos de Respiradores. Pruebas de Seguridad Y Requisitos de Investigacion Clinica. Available online: https://www.aemps.gob.es/informa/notasInformativas/productosSanitarios/2020/NI-PS_11-2020-respiradores-pruebas-investigaciones.pdf?x33378 (accessed on 15 May 2023).
35. Specification for Ventilators to Be Used in UK Hospitals during the Coronavirus (COVID-19) Outbreak. Available online: https://www.gov.uk/government/publications/specification-for-ventilators-to-be-used-in-uk-hospitals-during-the-coronavirus-covid-19-outbreak (accessed on 6 July 2023).
36. Center for Devices and Radiological Health. Enforcement Policy for Ventilators and Accessories and Other Respiratory Devices during the Coronavirus Disease 2019 (COVID-19) Public Health Emergency. Available online: https://www.fda.gov/regulatory-information/search-fda-guidance-documents/enforcement-policy-ventilators-and-accessories-and-other-respiratory-devices-during-coronavirus (accessed on 6 July 2023).
37. Especificaciones Técnicas de Dispositivos Médicos para la Gestión de Casos de COVID-19 en los Servicios de Salud—OPS/OMS | Organización Panamericana de la Salud. Available online: https://www.paho.org/es/documentos/especificaciones-tecnicas-dispositivos-medicos-para-gestion-casos-covid-19-servicios (accessed on 6 July 2023).
38. Beer, R.H.M.D.; Kuypers, M.H.; Holland, J.; Schotte, H. Strömungswiderstandsrohr für Gasströmungsmesser. Patent No. EP0331773A1, 13 September 1989.